HARVEY W. KO, JAMES W. SARI, and JOSEPH P. SKURA

ANOMALOUS MICROWAVE PROPAGATION THROUGH ATMOSPHERIC DUCTS

A multidisciplinary approach that examines the effects of anomalous tropospheric refraction on electromagnetic microwaves is presented. Effects such as surface ducting have been observed for decades, but the ability to describe detailed features such as propagation loss has been lacking. A code has been developed to deal with atmospheres that have both vertically and horizontally changing inhomogeneities of refractive index. Information derived from this approach is used to predict and analyze errors caused by transmission fading, duct trapping, and duct leakage in many microwave systems.

INTRODUCTION

The magic carpet, which transported anyone to any desired place, is a device commonly found in Eastern story telling. In the *Arabian Nights' Entertainment,* Scheherazade tells of a carpet used by Prince Hussein to deliver a lifesaving elixer to Princess Nouronnihar instantly. In the *Koran,* an enormous carpet of green silk moved King Solomon, his court, and his armies on command.[1]

What we hear as folklore or fable often originates as an experience of physical reality. Therefore, as high technologists, we make an effort to rationalize strange occurrences with our understanding of science. Refraction, or the bending of the direction of electromagnetic waves, is responsible for many optical illusions usually found in hot environments where warm air can remain aloft over a cooler surface. Therefore, it is not surprising that the tales of a magic carpet or a flying horse coincide with sweltering Eastern regions such as Saudi Arabia, Iran, and India, all of which border on bodies of water, namely, the Red Sea, the Persian Gulf, and the Arabian Sea, respectively. A mirage is not a bewildering event to today's technologist; its physical existence is unquestioned.

Since we know that light encompasses only a small part of the electromagnetic spectrum, we realize that peculiar refraction effects should occur in other parts of the electromagnetic spectrum as well (Fig. 1). Pre-World War II tales of VHF radio transmissions reaching abnormally long distances (in excess of 2000 miles) are explained today in terms of the refraction of the waves by elevated tropospheric layers. Early VHF radar observations in 1944 allowed the coast of Arabia, from the Strait of Hormuz up through the Persian Gulf, to be depicted in detail from a radar located near Bombay, India – over 1700 miles away.[2]

The increased use of microwave and millimeter wave electromagnetic systems is leading to new tales of peculiar behavior that are becoming the folklore

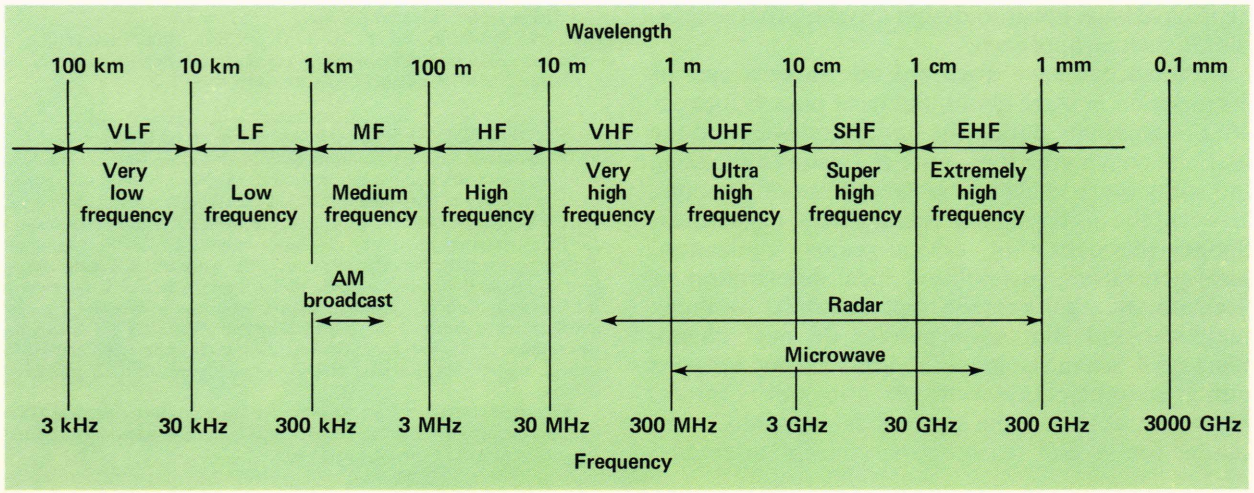

Figure 1 — The electromagnetic spectrum at radio frequencies.

of today. They will remain in this category until several technological disciplines such as boundary layer physics, meteorology, physical oceanography, and electromagnetic wave propagation are combined analytically and empirically to provide suitable explanations. This article reviews an analytical treatment of electromagnetic wave propagation near and inside tropospheric ducting layers, which are one cause of anomalous propagation.

TROPOSPHERIC REFRACTION

Over the frequency range shown in Fig. 1, the index of refraction, n, is essentially independent of frequency. The radio refractivity, N, is related to n by

$$N = (n-1) \times 10^6 \qquad (1)$$

and is a more convenient quantity. N may be determined empirically at any altitude from a knowledge of the atmospheric pressure, P, the temperature, T, and the partial pressure of water vapor, e, by

$$N = 77.6 \frac{P}{T} + 3.73 \times 10^5 \frac{e}{T^2} , \qquad (2)$$

where P and e are in millibars and T is in kelvin. The partial pressure of water vapor is proportional to the relative humidity, RH (in percent), and is given by

$$e = e_s \times RH ,$$
$$e_s = 6.1 \exp\left(25.22 \frac{T-273}{T} - 5.31 \ln \frac{T}{273}\right) , \qquad (3)$$

where e_s is the saturated vapor pressure in millibars.

In the standard atmosphere, temperature, pressure, and partial pressure of water vapor diminish with height in a manner that causes the index of refraction and radio refractivity also to diminish with height. The dependence of refractivity on temperature and relative humidity can be examined with the help of Fig. 2. Refractivity calculated from Eqs. 2 and 3 is plotted as a function of temperature for two values of pressure.

The curves are parameterized to four values of relative humidity. The upper set of curves is for P = 1013 millibars, which corresponds to sea level; the lower set of curves is for P = 795 millibars, which corresponds to an altitude of 10,000 feet. At colder temperatures, the contribution of water vapor to refractivity is small because the saturated vapor pressure (Eq. 3) is small. However, at higher temperatures, humidity plays an increasingly important role in refraction.

At optical frequencies, there is generally no such dependence of the refraction on humidity. While the

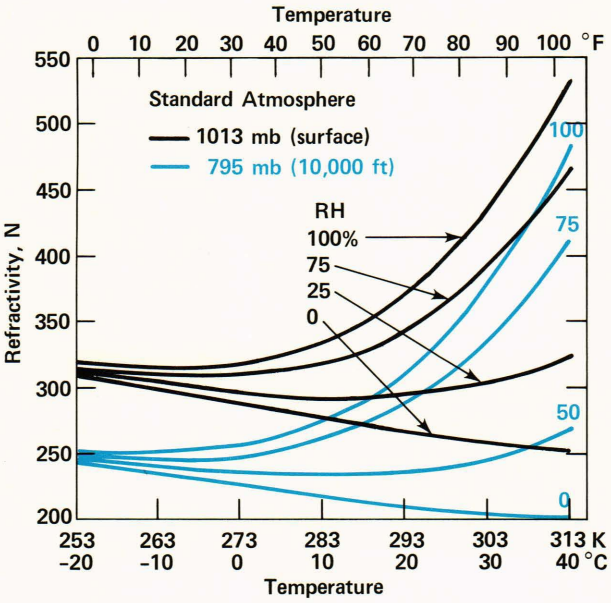

Figure 2 — The dependence of the refractivity, N, on temperature and humidity in a standard atmosphere. Atmospheric pressure levels are 1013 millibars (black) at the surface and 795 millibars (red) at 10,000 feet altitude.

electric dipole moment of water molecules can be reoriented by radio and radar frequency electric fields, it cannot follow the more rapidly alternating electric field at optical frequencies. Therefore, such peculiar optical refractive effects as mirages may not be caused by the same physical phenomenon that causes similar anomalous refractive effects at radar frequencies.

The condition of the atmosphere for electromagnetic propagation purposes can be assessed by examining the vertical profile of refractivity. The basic values of temperature, pressure, and relative humidity can be derived from radiosonde measurements. Under standard conditions at which electromagnetic rays travel normally, the refractivity profile will have a slope in the range of -24 to 0 N units per thousand feet. In our everyday perception of height, range, and distance, we find that normal propagation means that an electromagnetic ray launched horizontally will bend slightly downward toward the surface with a ray curvature about twice that of the earth's radius. This bending down is the consequence of the refractivity decreasing with height and can be rationalized with the use of Snell's law. Generally, in atmospheres with relatively simple refractivity changes, ray-tracing techniques based on Snell's law can be used to describe ray paths through the atmosphere. A modified refractivity, M, is defined as

$$M = N + \left(\frac{h}{r}\right) , \qquad (4)$$

where h is the height above the earth's surface at which M is derived and a is the earth's radius. M in-

cludes both atmospheric refraction and the effects of the earth's spherical curvature. Therefore, when the vertical gradient, dM/dz, is zero at any height, the path of a ray launched horizontally is a circular arc parallel to the earth's surface. [3]

Anomalous refraction is grouped into three major categories that can be understood with the help of Fig. 3. Relative to normal propagation paths, subrefraction is the bending up of rays, superrefraction is the bending down of rays, and trapping is the severe bending down of rays (with a radius of curvature much less than the earth's). In the case of trapping, rays may be guided by the earth's surface or by other layers of grossly different index of refraction. Figure 4 gives the index gradient changes of refractivity and modified refractivity profiles for these three types of anomalous refraction. Another virtue of the modified refractivity index is that potential trapping is easily identified whenever dM/dz is zero or less.

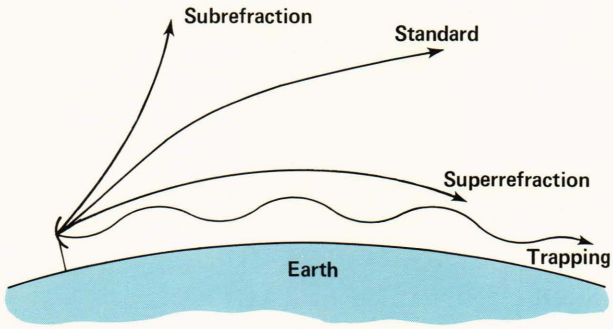

Figure 3 — Three basic categories of anomalous propagation in the troposphere.

TROPOSPHERIC DUCT PROFILES

Three common duct types are described in simple fashion in Fig. 5 with straight-line segment modified refractivity (M) profiles. The evaporation duct is typified by a negative value of dM/dz adjacent to the surface. The height of the duct, D is given by the vertical position of the M-profile inflection point, where dM/dz changes from a negative value (or zero) to a positive value. Rays launched inside the duct, with ray directions within a few degrees of parallel with the duct boundaries, will be trapped. Precisely how small these shallow or small grazing angles need to be for trapping to occur is dependent on the wavelength of the radiation, the vertical dimension of the duct, and the strength of the duct (as gauged by the dM/dz gradient). Figure 6 illustrates typical ray paths if launched horizontally (a), at various angles from the surface (b), or at various angles from above an evaporation duct (c).

The evaporation duct is found regularly over relatively warm bodies of water. It is generally caused by a temperature inversion near the surface (i.e., where temperature increases with height) and is accentuated by the intense relative humidity near the surface caused by water evaporation. Inspection of Fig. 2 shows the rapid change of the radio refractivity (N)

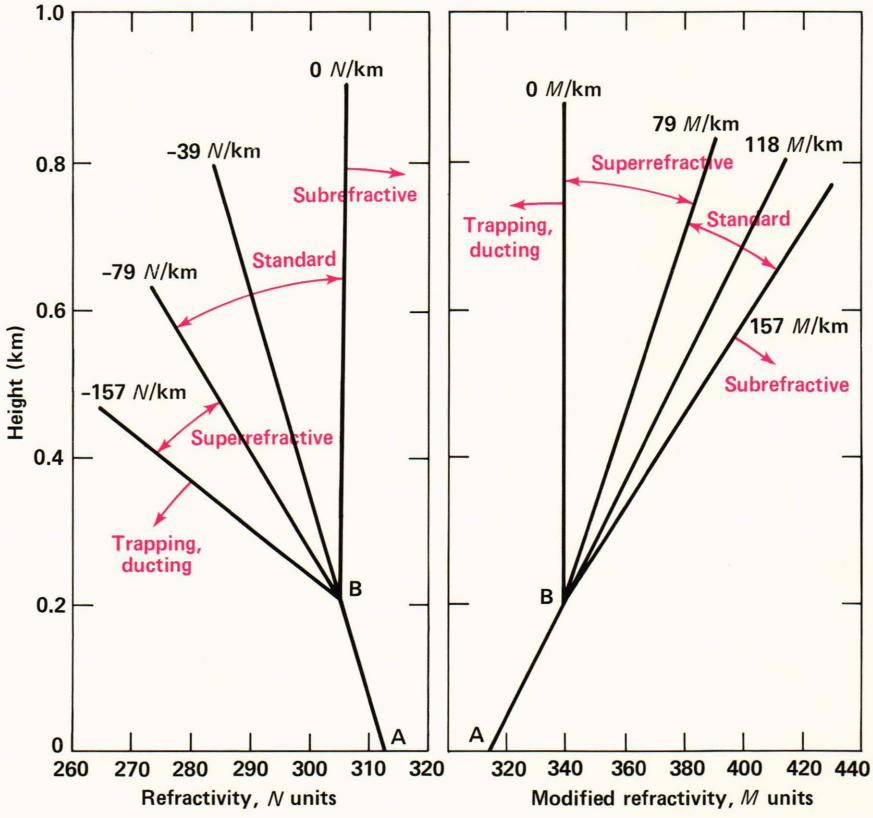

Figure 4 — Vertical profiles of refractivity, N, and modified refractivity, M, showing the range of profile slopes that classify the three basic categories of anomalous propagation.

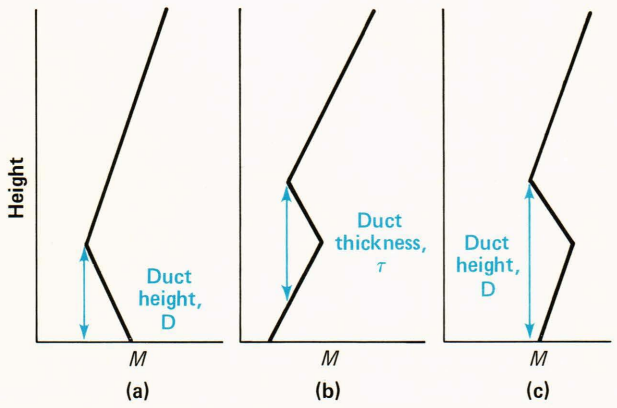

Figure 5 — Stylized vertical profiles of modified refractivity, *M*, identifying the presence of the (a) evaporation duct, (b) elevated duct, and (c) surface-based elevated duct.

for the higher temperatures and for relative humidity above 75%.

Over land surfaces, a duct with the profile of Fig. 5a can be formed in situations when an intense layer of low-lying humidity is found over a surface that is cooling more rapidly than the surrounding air (e.g., fog). This type of duct can also be found over land surfaces when the relative humidity is low but there is a tremendous daytime temperature inversion over a locally cool surface caused by intense air temperature from heat reradiated from surrounding surfaces (e.g., over a gray concrete runway surrounded by black asphalt). In this situation, it is better to speak of a surface duct rather than an evaporation duct, even though both ducts are typified by Fig. 5a.

An elevated duct is identified from a profile that contains an inflection point above the surface, accompanied by a modified refractivity value that is larger than the surface *M* value. Elevated ducts are caused primarily by temperature inversions aloft. These inversions can be caused by the intrusion of hot air into the region, or by the sinking or subsidence of air under high pressure centers. A faster-than-normal decrease of humidity with height usually accompanies these elevated inversions.

The thickness of the elevated duct, τ, is shown by the dotted lines in Fig. 5b. Rays launched at shallow angles into the vertical region of negative dM/dz will be trapped. Rays launched into the vertical region within τ, where dM/dz is positive, will be trapped only if they are horizontal. Rays launched at other than horizontal angles into this region will escape. Figure 7 illustrates the paths in the vicinity of an elevated duct from horizontally launched rays.

A surface-based elevated duct is present when the modified refractivity (*M*) value at the surface is lower than that at the lower inflection point, but not as low as that at the upper inflection point of a negative dM/dz region. The height of the surface-based elevated duct is shown in Fig. 5c. Rays launched horizontally into the region with positive dM/dz inside the height D will be trapped. Nonhorizontal rays in this region will escape. Rays launched at shallow angles into the region of negative dM/dz will be trapped.

BOUNDARY LAYER ALTERATION OF ELEVATED DUCTS

In coastal regions, thermal and mechanical effects can influence the tropospheric circulation and distribution of moisture, thereby affecting the electromagnetic index of refraction. Important mesoscale meteorological flows of concern are the land and sea breezes. The land and sea breezes are phenomena generally experienced when the land is subjected to considerable heating, and a large temperature differential develops between land and water. The juxtaposition of contrasting thermal environments results in the development of horizontal pressure gradient forces that, if sufficient to overcome the retarding influence of friction, will cause air motion across the boundary between the surfaces. Land and water surfaces possess contrasting thermal responses because of their different properties and energy balances, and this is the driving force behind the land and sea breeze circulation system.

These land-water temperature differences and their diurnal reversal (by day, land warmer than water; at night, land cooler than water) produce corresponding land-water air pressure differences. These differences in turn result in a system of breezes across the shoreline that reverses its direction between day and night. The daytime sea breeze circulation has a greater vertical and horizontal extent, and its wind speeds are higher than those in the nocturnal land breeze. During the sea breeze, the cooler and more humid sea air advects across the coast and wedges under the warmer land air. The advancing sea breeze front produces uplift in what is already an unstable atmosphere over

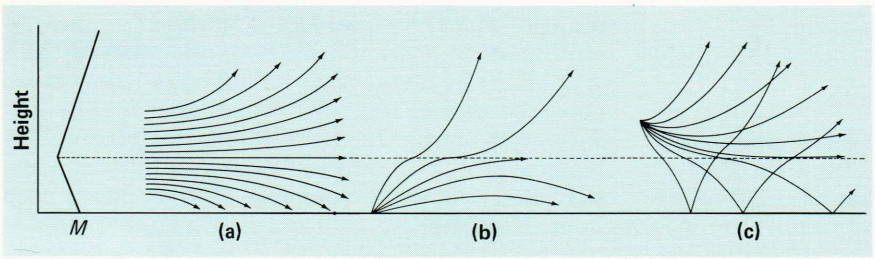

Figure 6 — Ray paths about an evaporation duct for rays (a) launched horizontally above and below the top of the duct, (b) launched upward at various angles from the surface, and (c) launched downward at various angles from above the duct.

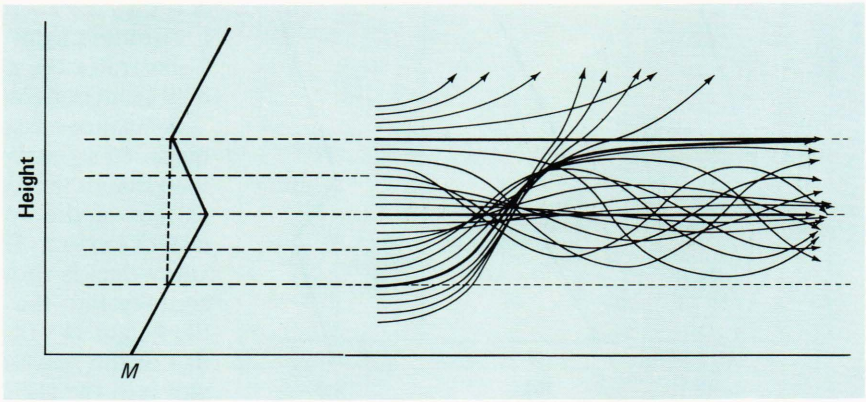

Figure 7 — Paths about an elevated duct from horizontally launched rays.

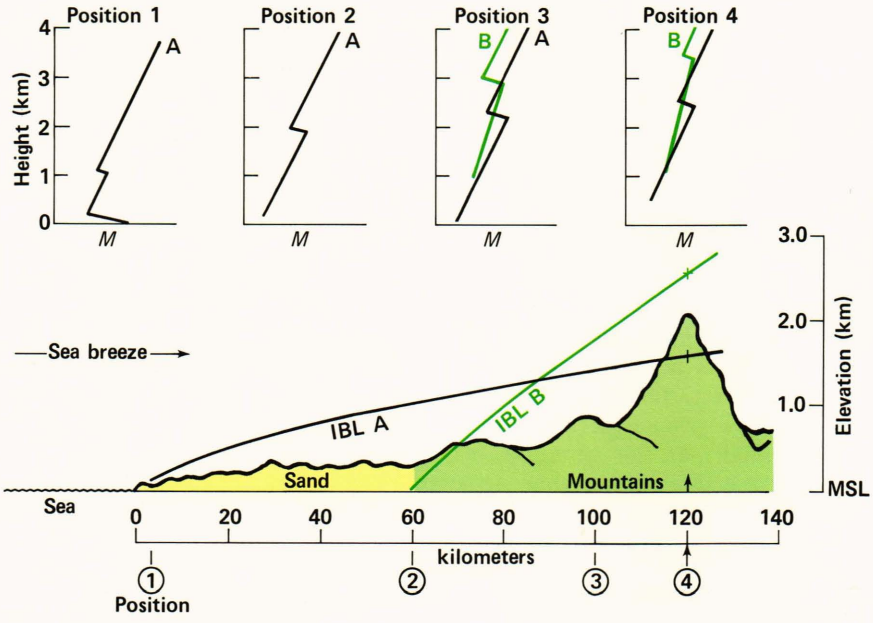

Figure 8 — A model for the daytime boundary layer alteration of elevated ducts over a coastal site. Two sea breeze internal boundary layers (IBL) are shown, each corresponding to a different value of surface roughness. The corresponding shift in the height of the elevated duct is shown in the *M*-profile at four locations.

the land. The stable marine air is warmed over the land, producing a more unstable internal boundary layer that grows in depth with time and distance from the shore. The nature of uplifting of anomalous refractive layers can be visualized with the aid of Fig. 8, which is a stylized representation of the daytime sea breeze condition. The colored curves illustrate the spatial change of the internal boundary layer whose height grows slowly with inland distance. The height of the boundary layer, H_B, can be calculated at each horizontal position, x, from the formula

$$H_B = z_2 [0.75 + 0.03 \ln (z_1/z_2)] (x/z_2)^{0.8} , \quad (5)$$

where z_1 and z_2 are the upwind (water) and downwind (land) surface roughness lengths, respectively.[4] This is an empirical relationship that has been found to be in reasonable agreement with measurements at various locations worldwide. As air passes from one surface type to a new and meteorologically different surface, it must readjust itself to a new set of boundary conditions. Therefore, two boundary layers are shown in Fig. 8: layer A for the sea-land surface transition, and layer B for the sand-mountain surface transition. Boundary layer A uses $z_1 = 10^{-3}$ centimeter (water) and $z_2 = 5 \times 10^{-2}$ centimeter (sand); boundary layer B uses $z_1 = 5 \times 10^{-2}$ centimeter (sand) and $z_2 = 10$ centimeters (mountains).

The concomitant alteration of index of refraction is illustrated in Fig. 8 with vertical profiles of the modified refractivity (M). At position 1, the presence of an elevated duct is indicated by the negative gradient of M and the local minimum M value at a height of about 2600 feet. By the time the sea breeze penetrates 70 nautical miles inland, the boundary layer uplifts the elevated duct to 7800 feet for boundary layer A, or to 10,000 feet for boundary layer B. Precisely which boundary layer applies is open to question because of the stylized nature of this M data extrapolation. Figure 8 is used here only for il-

lustrative purposes. Nevertheless, it is clear that electromagnetic wave propagation (e.g., from a site at 7000 feet elevation in the mountains [position 4] looking out to sea) can be complicated by horizontal as well as vertical inhomogeneities in refractivity.

INHOMOGENEOUS ELECTROMAGNETIC WAVE PROPAGATION

Most analyses of wave propagation through simple refractive changes in the atmosphere can be treated with geometrical ray-tracing techniques. For example, an atmosphere that is horizontally stratified, with anomalous layers described by piecewise linear segments of modified refractivity, does not present much of an analytical problem for geometrical optics if only ray directions are required. However, certain general limitations exist for ray-tracing methods: (a) the refractive index must not change appreciably in a distance comparable to a wavelength; (b) the spacing between neighboring rays must be small or questionable results occur when rays diverge, converge, or cross; (c) constructive and destructive interference is difficult to evaluate for more than one reflection from a surface; (d) the distance a ray may travel is difficult to evaluate without a method to compute propagation loss; and (e) diffraction phenomena are not accounted for in homogeneous media. Therefore, a physical optics approach, which can account for propagation loss and diffraction, is usually sought for most problems of sophistication. Until the advent of large-capacity computers and numerical algorithms like the fast Fourier transform, physical optics solutions to ducting problems relied on closed-form mathematical treatments. As with the ray-tracing methods, these approaches generally simplified the true atmosphere with horizontally homogeneous, linearly or logarithmically stratified index layers. Most solutions treated wave propagation in a fashion similar to waveguide analysis, using modal-type, separable differential equations.

As we see from the boundary layer alteration of elevated layers, many real-world situations cannot be discussed within the framework of a vertically stratified, horizontally homogeneous atmosphere. When refractive index changes (or equivalently, dielectric constant changes) are found to be inhomogeneous in both the horizontal and the vertical directions, the electromagnetic propagation equations are generally nonseparable and difficult to solve analytically. Several investigators[5] have approached this problem numerically via coupled-mode analysis using a cylindrical earth model and an infinite line source; horizontal inhomogeneities are considered by assuming horizontally piecewise uniform media. Modal analysis tends to be difficult, with the cost of computer time limiting convergent answers to simple refractive changes. The approach here for a numerical solution is to obtain for vertically and horizontally varying media an approximation to the propagation equation comparable to that obtained by Leontovich and Fock[6] for vertically inhomogeneous media.

An elliptic wave propagation equation is replaced by a differential equation of the parabolic type, after suitable approximation, which is dependent on wave frequency and refractive index strength and spatial distribution. The resultant equation may be solved with a marching-type numerical method called the split-step Fourier algorithm,[7] developed about 10 years ago for ionospheric propagation. The advantage of this approach is that it allows for complex two-dimensional inhomogeneous variations (i.e., not just linear or logarithmic, but also arbitrary profiles of the modified refractivity, yielding physical optic computations of transmission loss. The general limitations of this approach concern the absence of backscatter results and its restriction to use with relatively oblique propagation to the surface.

ANOMALOUS PROPAGATION EFFECTS FROM ELEVATED REFRACTIVE LAYERS

Many electromagnetic systems are susceptible to anomalous propagation problems caused by elevated layers. Antennas used for communications, telemetry, airplane instrument landing systems, and radar sets are prime candidates for such problems either because of their physical proximity to the anomalous elevated refractive layers or because their ray paths pass through the layers. The possibility of such errors can be intuitively understood with the help of Fig. 9.

The airborne radar in Fig. 9a incurs performance compromise from an elevated subrefractive layer and a warped elevated duct. Some rays from the airborne radar are severely bent upward, leaving a void in coverage just below the subrefractive layer. Other rays from the airborne radar couple to the elevated duct and are severely bent downward and trapped. Many of the trapped rays escape from the elevated duct because of the duct's accentuated curvature, but their diversion has left a void in coverage. These types of airborne radar problems are usually transient in nature because of the high speed of the airplane and its constantly changing geometry relative to the anomalous refractive layers.

In Fig. 9b the ground-based radar has many rays diverted by the elevated duct, leaving a large coverage hole. Thermal heating from the sun will induce a temporal change in height of the boundary layer. This is likely to cause the elevated duct to migrate up and down, thereby causing this type of coverage problem to vary in its severity according to the time of day.

The surface-ship radar in Fig. 9c has its pattern severely diverted downward because of the elevated duct. This behavior leaves higher elevation targets uncovered and causes excessive land clutter.

In addition to coverage holes and clutter, anomalous propagation can cause another severe error. A ray, diverted away from its intended direction, may detect a target. The radar system will indicate the

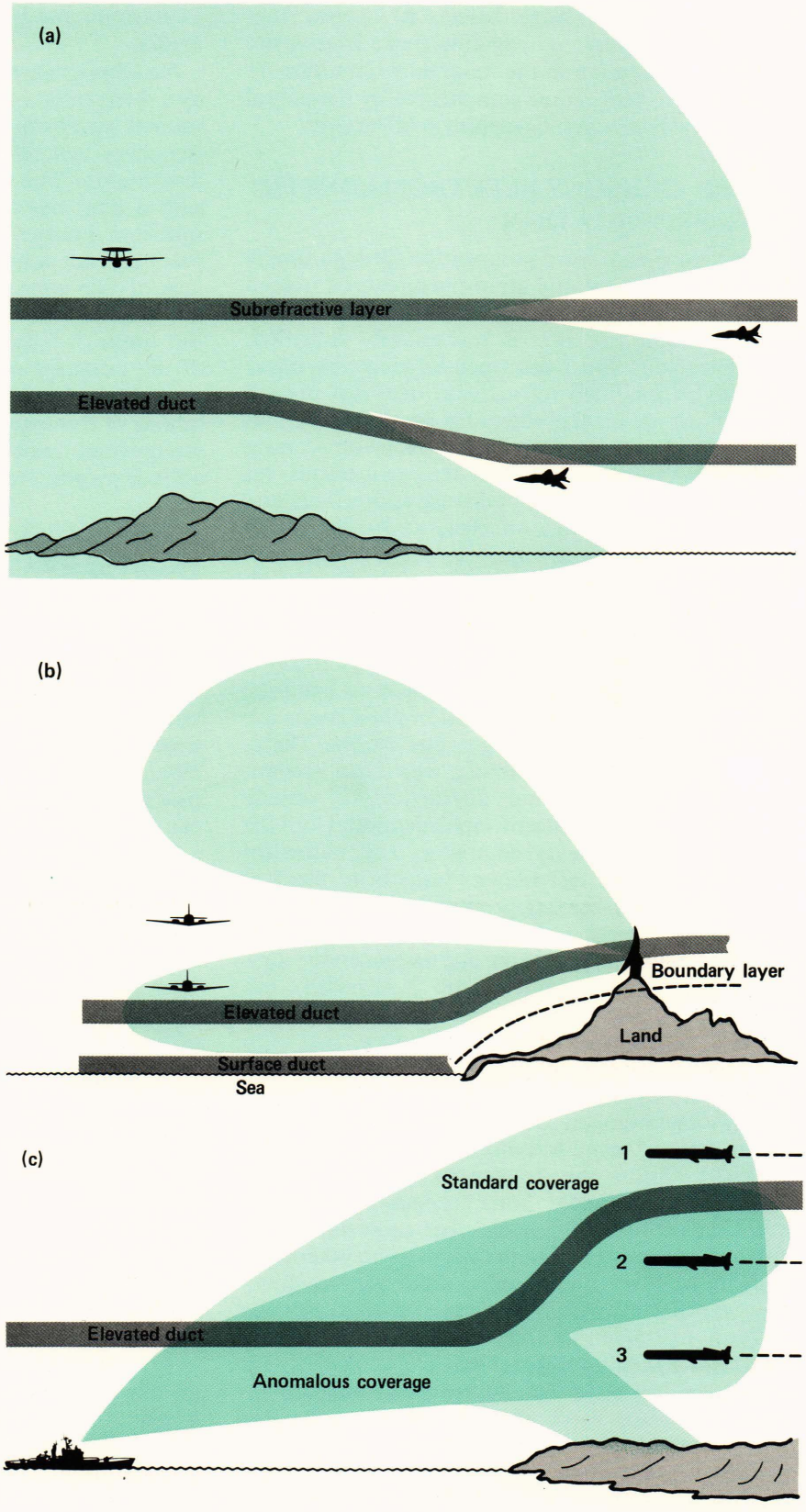

Figure 9 — Potential radar coverage problems from elevated anomalously refractive layers. These are based on computer simulations for a radar that is (a) airborne over 10,000 feet high, (b) ground-based at 7000 feet elevation, and (c) shipborne below 100 feet elevation.

target to be along the originally intended direction and at the wrong height. This is commonly called the height error.

With the help of the APL inhomogeneous propagation analysis, we can examine some of these situations in more detail. An example of this analysis is

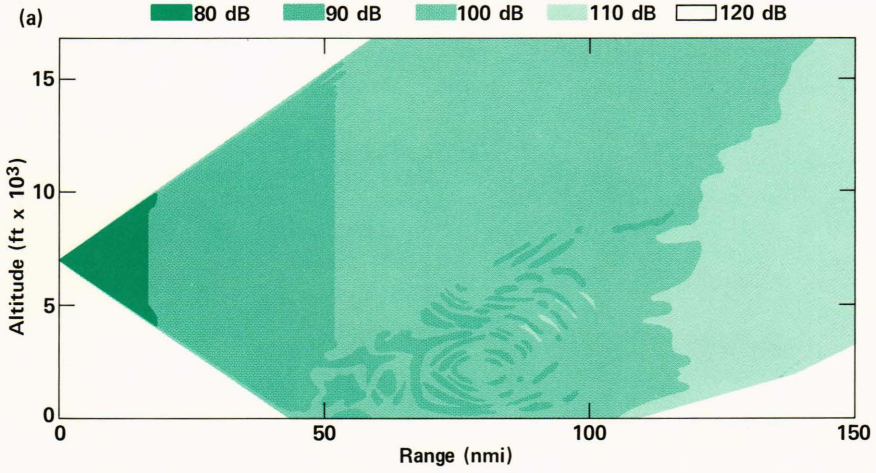

Figure 10 — Propagation loss is given for a 600-megahertz antenna pointed horizontally into a standard atmosphere. In (a) the loss in dB relative to 1 meter is mapped in vertical and horizontal coordinates. In (b) the vertical loss profile in dB relative to free space is given at several downrange distances. The 3° vertical beamwidth antenna is at 7200 feet elevation.

given in Fig. 10a, a diagram of transmission loss (in dB relative to 1 meter), geometrically plotted in range-height coordinates. An antenna at an elevation of 7200 feet with 0° elevation angle, 3° vertical beamwidth, horizontal polarization, and (sin x)/x pattern is used at 600 megahertz to propagate into a standard atmosphere. The earth's surface is perfectly conducting. General features that are clearly visible are the antenna pattern, the r^{-2} loss, and the constructive and destructive interference patterns caused by energy reflected off the earth's surface. Another method for examining the results is given in Fig. 10b where vertical profiles of transmission loss relative to free space are plotted at several horizontal ranges away from the antenna. Figure 10a gives an overall spatial summary of the transmission loss revealing spatial coverage. Figure 10b gives much more detail for the transmission loss at each altitude. Note the deep loss regions outside the antenna beamwidth and the over-the-horizon shadow region.

Figure 11a gives a spatial summary for a more complex situation. Here, the same antenna is now propagating into a situation closely mimicking the tropospheric conditions of Fig. 9b, a curved elevated duct. Initially, over the antenna position, the elevated duct is above the antenna at a height of 7400 feet, drops to a height of 2200 feet at a range of 64 nautical miles, and remains at 2200 feet to 250 nautical miles and beyond. The initial modified refractivity (M) deficit for the elevated duct over the antenna position is 136 M units. Figure 11a shows that large continuous voids are now present because of the transfer of energy down to the surface. These voids (120 dB), not formerly present in the standard atmosphere case, are located near the antenna just above the elevated duct and at increasingly higher elevations away from the antenna, even above the normal line of sight. Thus, severe compromises in vertical coverage are revealed that are not predicted by homogeneous propagation calculations. Figure 11b gives the vertical profiles of transmission loss relative to free space for the same conditions. This figure reveals more information, such as loss within the duct and increased energy at the surface beyond 150 nautical miles (thereby possibly introducing anomalous sea clutter).

At higher frequencies, the coverage holes caused by anomalous propagation tend to be spatially larger and deeper in loss. Figure 12 illustrates the behavior at high frequencies for the curved elevated duct. The antenna is situated at 7000 feet. The antenna characteristics used are 1.2 gigahertz, (sin x)/x pattern, 5° vertical beamwidth, 0° elevation angle, and horizontal polarization. If one imagines the curved elevated duct to be a "carpet" lying across the coastline with a curvature of the boundary layer, then the anisotropy of propagation along different azimuthal directions is apparent.

The result for propagation along the direction of maximum curvature (or maximum inhomogeneity) is shown in Fig. 12a. The curvature is the same as that used for Fig. 11; however, as opposed to the previous situation, the elevated duct is intersecting the radar antenna at the site. The maximum height of the elevated duct is shown by the dashed line. Several sig-

The Parabolic Approximation For Inhomogeneous Electromagnetic Wave Propagation

A well-known approximation, the "parabolic approximation," was obtained by Leontovich and Fock in 1946[A1] for propagation in a vertically inhomogeneous, horizontally homogeneous atmosphere over a spherical earth. An extension of this approach[A2] for a horizontally and vertically inhomogeneous atmosphere begins with the spherical earth geometry shown in Fig. A1. The inhomogeneities in the atmospheric dielectric constant, ϵ, are modeled in terms of variations in the radial and polar angle directions, $\epsilon = \epsilon(r,\theta)$. Azimuthal symmetry in ϵ is assumed about the origin of the field situated at the pole. The consequence of assuming azimuthal symmetry is that the variations in the atmospheric dielectric constant are limited to two dimensions; in a practical sense this assumption greatly simplifies the mathematics. In the geometry shown in Fig. A1, the source field is assumed to originate from a raised vertical electric dipole (VED) situated at the pole; this assumption also is for mathematical simplification. The resultant approximate equation governing propagation, however, will be the same if a horizontal electric dipole (HED) source were assumed; only the boundary conditions to be satisfied at the earth's surface will differ.

Because of the VED source and the assumed symmetries, only the vector field $\vec{E}_r$, $\vec{E}_\theta$, and $\vec{H}_\phi$ exist. One can find a scalar equation for the magnetic field, $\vec{H} = H(r, \theta)\vec{1}_\theta$, by combining Maxwell's equations to eliminate the electric fields:

$$-\vec{\nabla} \times \vec{\nabla} \times \vec{H} + \omega^2 \mu \epsilon \vec{H} = -\frac{\vec{\nabla}\epsilon}{\epsilon} \times (\vec{\nabla} \times \vec{H}). \quad \text{(A1)}$$

The magnetic permeability, μ, is constant, and the electric field can be obtained similarly. Generally, one is interested in examining variations in the fields, which are relatively long compared to a wavelength. One expects, however, that along the earth's surface in the horizontal direction from the source, the fields will oscillate like e^{iks} (where k, the wavenumber, equals $2\pi/\lambda$). Therefore, it is reasonable to factor this rapidly oscillating behavior out of the solution. A convenient substitution that factors out rapid oscillating behavior as well as large variations near the source, and a linear trend in radius, is obtained in terms of an attenuation function $U(r, \theta)$ defined by

$$H(r,\theta) = \frac{U(r,\theta)}{r} \sin\theta^{-1/2}\, e^{-1}\, e^{ik_o a\theta}. \quad \text{(A2)}$$

Here $k_o^2 = \omega^2\mu\epsilon\ (a, 0) = \omega^2\mu\epsilon_0$ is the square of the electromagnetic wavenumber at the earth's surface, $r = a$.

A good deal of mathematics ensues as Eqs. A1 and A2 are combined into a propagation equation for $U(r, \theta)$, which is an elliptic differential equation in the horizontal and vertical directions. For values of ϵ in the troposphere, and for wavelengths much smaller than the scale of change of ϵ, many terms in this equation can be ignored to obtain

$$\frac{\partial^2 U}{\partial h^2} + \frac{2ik_0}{a}\frac{\partial U}{\partial \theta} + k_0^2\left[\frac{\epsilon(h,\theta) - \epsilon_0}{\epsilon_0} + 2\frac{h}{a}\right]U = 0, \quad \text{(A3)}$$

which is a parabolic differential equation that is second order in the vertical direction and first order in the horizontal direction.

In obtaining Eq. A3, the radial coordinate has been transformed into $h = r - a$, where h is the height above the earth's surface. The effect of the atmospheric inhomogeneities are contained in $\epsilon(h, \theta)$. If the horizontal direction along the earth's surface is defined as $s = a\theta$, Eq. A3 can be thought of as representing propagation above a flat earth. The effect of a spherical earth is accounted for by an effective linear gradient in the index of refraction, $2h/a$; this approximation, using a linear gradient, is good for tropospheric altitudes $h << a$. The treatment of a spherical earth by means of a linear gradient in ϵ is conveniently handled by converting the refractivity index, N, into the modified refractivity index, M, as has been discussed in the text.

The conditions that must be satisfied so that the original elliptic equation may be approximated by the parabolic Eq. A3 are summarized as follows:

$$\text{(a)}\quad \frac{1}{\epsilon}\frac{\partial \epsilon}{\partial s} \lesssim 10^{-2} k_0,$$

$$\text{(b)}\quad \theta \geq 10^2 (k_0 a)^{-1}, \quad \text{(A4)}$$

$$\text{(c)}\quad k_0 a \frac{\partial U}{\partial \theta} \gg \frac{\partial^2 U}{\partial \theta^2},$$

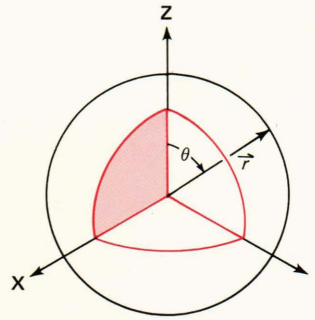

Figure A1 — Spherical earth-vertical electric dipole geometry.

$$\text{(d)} \quad \frac{1}{\epsilon}\frac{\partial \epsilon}{\partial h} \ll \left(\frac{2k_0^2}{a}\right)^{1/3} .$$

If one associates

$$\epsilon \left| \frac{\partial \epsilon}{\partial s} \right|^{-1}$$

and

$$\epsilon \left| \frac{\partial \epsilon}{\partial h} \right|^{-1}$$

with the radii of curvature of rays resulting from horizontal and vertical variations in ϵ, then conditions (a) and (d) require that these radii be large compared with a wavelength. That is, the horizontal and vertical variations in ϵ must be reasonably slow; for situations of interest in this article, this requirement holds. Condition (b) implies that reasonable values will be obtained for distances greater than 100 wavelengths from the source. Finally, condition (c) requires that the propagation be relatively oblique; that is,that rays be launched with low grazing angles ($\lesssim 20°$).[A3]

Solutions to the parabolic equation will be obtained if the initial source field is specified and the values of the field at the earth's boundary surface and ionosphere are properly defined. For simplicity, a nonreflecting or fully absorbing boundary is assumed at the ionosphere. For the surface boundary condition, a smooth-conducting earth is assumed; further, it is reasonable to assume that the skin depth of radiation within the earth is small compared to the earth's radius of curvature. In that case, the earth's curvature can be ignored and Leontovich's impedance boundary condition[A4] may be applied. If η_s is the complex dielectric constant of the earth, the boundary condition on $U(r, \theta)$ will be satisfied for a VED if

$$\frac{\partial U}{\partial r} + \frac{ik\epsilon_s}{\sqrt{\eta_s}} U = 0, \text{ at } r = a . \qquad \text{(A5)}$$

For a VMD source, the boundary condition on $U(r, \theta)$ will be

$$\frac{\partial U}{\partial r} + ik\sqrt{\eta_s}\, U = 0, \text{ at } r = a . \qquad \text{(A6)}$$

Practically speaking, vertical symmetric and antisymmetric solutions of U above the surface must be combined to satisfy either Eq. A5 or Eq. A6. However, if the earth's surface is approximated by a perfect conductor, Eqs. A5 and A6 reduce to the requirement that either $(\partial U/\partial r)$ (VED) or $U = 0$ (VMD) at the surface. In those cases, one need obtain only symmetric (VED) or antisymmetric (VMD) vertical solutions about the surface, and these boundary conditions are automatically satisfied.

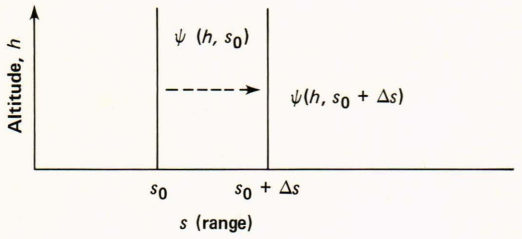

Figure A2 — Split-step algorithm.

A number of numerical techniques exist for solving the parabolic equation. One technique that uses the computation speed of the fast Fourier transform is the split-step Fourier algorithm developed by Hardin and Tappert.[A5] The basis of the split-step algorithm is illustrated in Fig. A2. A source field that satisfies the appropriate boundary condition is assumed to be known as a function of altitude, h, at an initial range step, s_0. An approximate solution to the parabolic equation for all altitudes, h, at a greater range, $s_0 + \Delta s$ may be generated by first obtaining the Fourier transform, $\psi(p, s)$, of the source field distribution in the vertical direction, h. Similarly, if one takes the Fourier transform of the parabolic equation in the vertical direction, the resultant equation for the transformed field is first order in the horizontal direction:

$$-p^2\psi + 2ik_0 \frac{\partial \psi}{\partial s} + K^2\psi = 0 . \qquad \text{(A7)}$$

An exact solution to Eq. A7 is obtained if the propagation constant, K^2, is assumed to be relatively constant over a small step size, Δs. Then, as shown in Fig. A2, an updated, approximate solution to the field at $s_0 + \Delta s$ is obtained by an inverse Fourier transform where the variation in the propagation constant is applied outside the inverse transform:

$$\psi(h, s_0 + \Delta s) = e^{iK\Delta s/2}\, FT^{-1} \times [e^{-i\Delta s p^2/2k_0}\, \psi(p, s_0)] , \qquad \text{(A8)}$$

where p is the transform variable. The error in this approximation solution varies to some power of the step size, and stable solutions are obtained with stability generally depending on step size. The solution for the fields for arbitrary ranges are obtained in an identical manner for each step by using the field solution at each new range step as the initial condition for generating the solution at the subsequent range step. For this numerical solution, two fast Fourier transforms are required for each step.

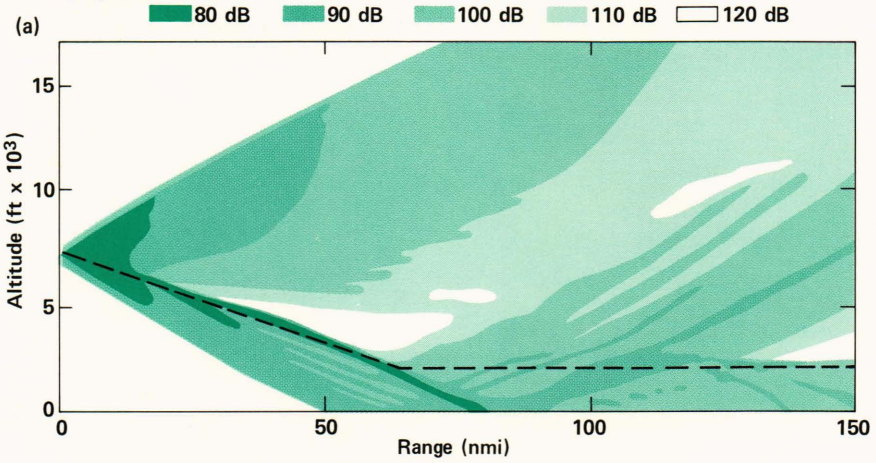

Figure 11 — The same 600-megahertz antenna of Fig. 10 is pointed horizontally into an atmosphere with a curved elevated duct (dashed line). In (a) the loss in dB relative to 1 meter is mapped in vertical and horizontal coordinates. In (b) the vertical loss profiles are given in dB relative to free space. Huge losses leading to coverage holes are seen in each display.

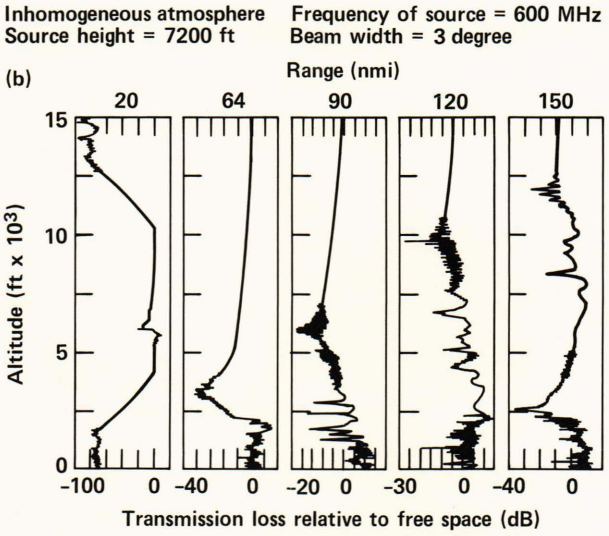

nificant results are shown. There are several void regions (not just the one predicted by ray tracing); energy is not trapped in the duct, but escapes because of the large duct curvature; and excessive energy is diverted down to the surface. At the same time, along a direction of less curvature (or less inhomogeneity), different features are shown in Fig. 12b. New voids at high altitude are seen because of the waves' inability to "burn through" the elevated duct. Aside from the obvious problem of radar holes, these features could cause significant fading and bit-error rates for air-to-air telemetry links as well. Also note that waves are trapped and guided by the elevated duct and not diverted to the surface as in Fig. 12a. Unlike the results from ray tracing, these physical optics results show multiple void structure and give the propagation loss everywhere, especially inside the duct.

PROPAGATION LOSS ABOUT EVAPORATION DUCTS

A common problem for shipborne radar systems is trapping by the evaporation duct. The height and strength of the evaporation duct vary from one geographical location to another. Seasonal and diurnal influences present at each locale regularly change the duct character. In the summertime, the duct height over the North Atlantic might be 50 feet, which is relatively low compared to the duct height over the Persian Gulf, which may be 300 feet. Therefore, a radar antenna on a ship in the North Atlantic is likely to operate at an elevation that is usually within or above the duct. The usual perception of shipborne radar ducting is shown in Fig. 13. Figure 13a depicts normal coverage, which usually extends to about 250 nautical miles under standard atmospheric conditions. For a 100-foot antenna height, the radar horizon is 12.3 nautical miles. Neglecting diffraction, no energy is transmitted below the line of sight that passes through the antenna and the radar horizon. In the presence of a horizontally homogeneous evaporation duct (Fig. 13b), energy is trapped and guided near the surface well beyond the horizon. This ducting diverts rays away from normal coverage, leaving a large region at the far end of the pattern that will not be covered by the radar. Also, a wedge-shaped hole in the coverage extends from the far end of the pattern back to the antenna with a vertical gap that can be on the order of 1000 feet thick at a range of 100 nautical miles.

Simulations accounting for horizontally inhomogeneous situations are now admitting new possibilities for radar behavior about the evaporation duct. In Fig. 13c the evaporation duct height is gradually diminishing at increasing ranges from the ship. Energy initially trapped by the duct is now leaking out of the duct at downrange distances. Trapped waves do not propagate as far over the horizon as they do in the case of the homogeneous duct. Further, the wedge-shaped hole in coverage consists of a larger vertical gap.

Details of the propagation loss can be examined in Fig. 14, which plots the dB loss relative to 1 meter in horizontal and vertical dimensions. The standard atmospheric (a) and the homogeneous duct (b) situations are studied in a range of 0 to 100 nautical miles for altitudes from 0 to 1000 feet. A $(\sin x)/x$ antenna

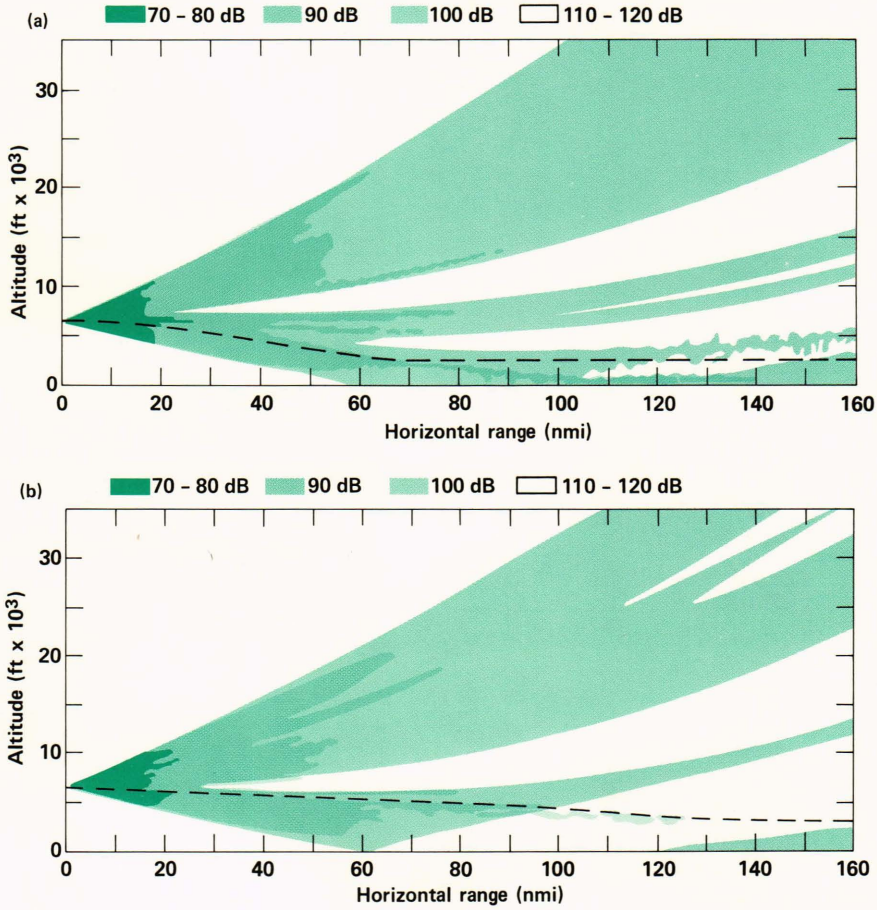

Figure 12 — Propagation loss in dB relative to 1 meter is mapped for a 1.2-gigahertz antenna pointed horizontally into an elevated duct (dashed line). Along the direction of maximum duct curvature (a), energy is diverted to the surface. Along a direction of slight duct curvature (b), the same duct traps energy to extended range.

pattern, with 0° elevation and 2° vertical beamwidth, is used at 3 gigahertz, and the antenna is placed at a 100-foot height. The homogeneous duct has a duct height of 50 feet and linear refractivity gradients of -200 N units per thousand feet inside the duct and -21 N units per thousand feet above the duct. In spite of the antenna's position 50 feet above the duct, the finite antenna beamwidth allows some waves to be trapped, extending coverage near the surface. Note that the 90-dB loss level at the surface extends to the 12.3-nautical-mile range in the standard situations; this level is extended to about 40 nautical miles in the homogeneous duct case. In general, the duct extends coverage for targets between the surface and 1000 feet, but the wedge-shaped gap appears and excess surface clutter is predicted.

If the height of the duct is allowed to drop linearly from a height of 50 feet at the antenna position to a height of 30 feet at 100 nautical miles downrange, the coverage changes slightly, as seen in Fig. 15a. The duct strength is held at -200 N units per thousand feet. In both duct cases, the extent of trapping is slight because only a few antenna rays couple to the trapping layer. However, if the duct height is allowed to rise, more rays enter the duct and severe trapping occurs. This is seen in Fig. 15b, for which the same antenna is placed above a duct whose height rises linearly from 50 feet at the antenna position to 100 feet

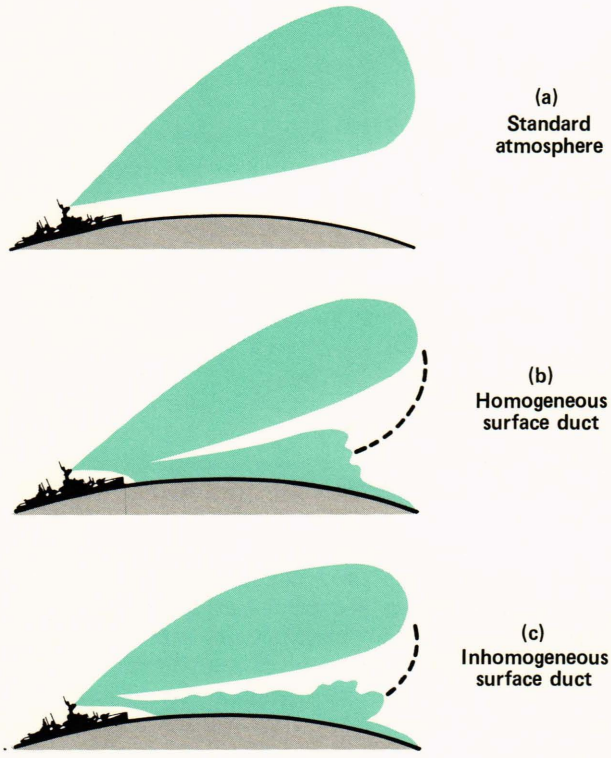

Figure 13 — Shipborne radar coverage in the presence of (a) standard, (b) homogeneous evaporation duct, and (c) inhomogeneous evaporation duct environments.

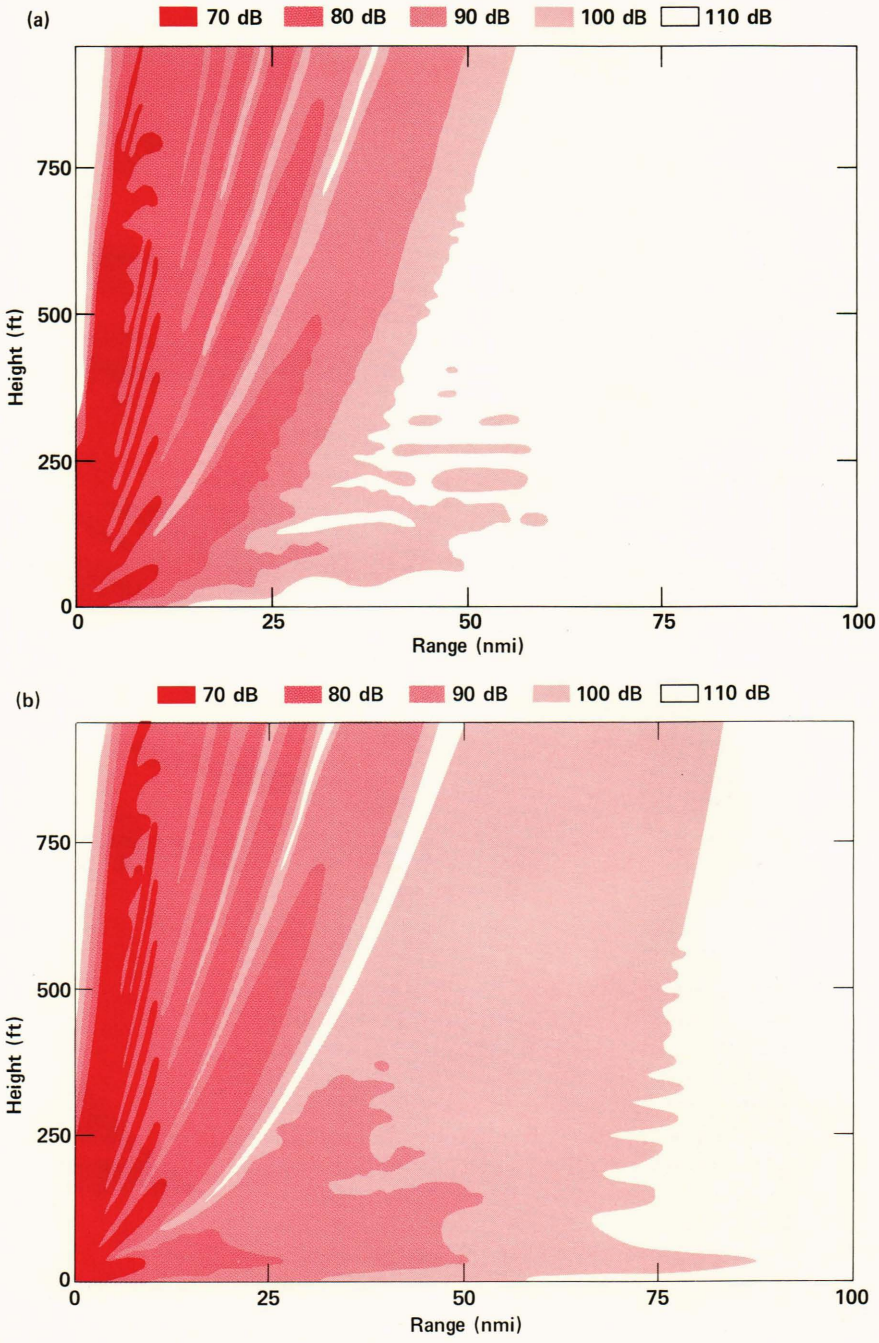

Figure 14 — Propagation loss for a 3-gigahertz antenna at 100 feet elevation (a) in the standard atmosphere and (b) above a homogeneous evaporation duct with a 50-foot height.

at 100 nautical miles downrange. The duct strength is held at -200 N units per thousand feet. Significant energy at the 90-dB loss level is sustained near the surface well beyond the 100-nautical-mile range.

Further detail is provided by Fig. 16, where the propagation loss in dB relative to 1 meter is provided as a function of downrange distance from the antenna for the three duct cases (constant height, diminishing height, increasing height). Results are given for an altitude of 40 feet either within or near the ducts, and altitudes of 100 feet, 500 feet, and 900 feet above the ducts. At a 100-nautical-mile range for the 40-foot altitude, 20 dB more power than the homogeneous duct is present in the inhomogeneous duct with rising height; 30 dB less power than the homogeneous duct is present in the inhomogeneous duct with falling height. At ranges between 30 and 70 nautical miles, examination of the loss at the other altitudes shows significantly less power for the rising-height duct case than either the constant-height or falling-height duct cases because of the excessive energy trapped in the duct itself. Another important feature present in the rising-duct case at these altitudes is the spatially periodic fading.

Clearly, different duct environments will cause different trapping features to arise. Further investiga-

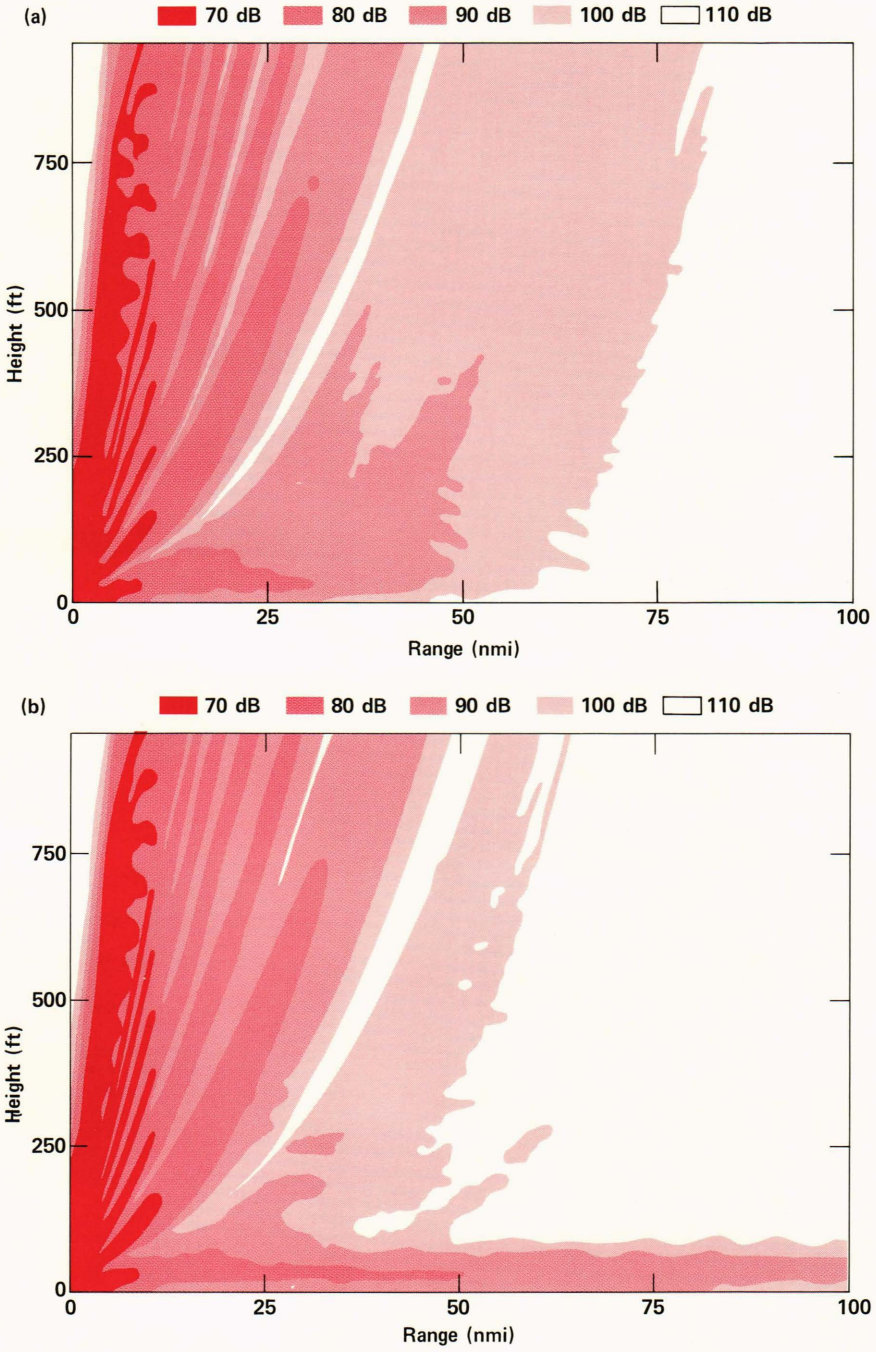

Figure 15 — Propagation loss for a 3-gigahertz antenna at 100 feet elevation above inhomogeneous evaporation ducts with (a) height diminishing downrange from 50 feet to 30 feet, and (b) height increasing downrange from 50 feet to 100 feet.

tions are needed to catalog the dependence of coverage void and propagation loss structure on duct height, duct strength, frequency, and antenna characteristics. It is wise not to formulate a stereotyped understanding of evaporation duct behavior.

CONCLUDING REMARKS

It is well accepted that anomalous propagation affects the performance of many electromagnetic systems, some of which are radar surveillance, communications and data link, airplane instrument landing, navigation and tracking, weapons fire control, electronic countermeasures and counter-counter-measures, and signal intelligence. The word anomalous is meant to be synonymous with nonstandard. However, too often the misleading connotation of infrequent occurrence is attached. Until recently, this misunderstanding stemmed primarily from the lack of a rational, scientifically based explanation that could interpret or predict the peculiar behavior. As systems become more sophisticated and as more precision is required, a better understanding of anomalous propagation is sought.

Several technical disciplines are being combined for this purpose. Electromagnetic wave propagation formulations continue to address propagation

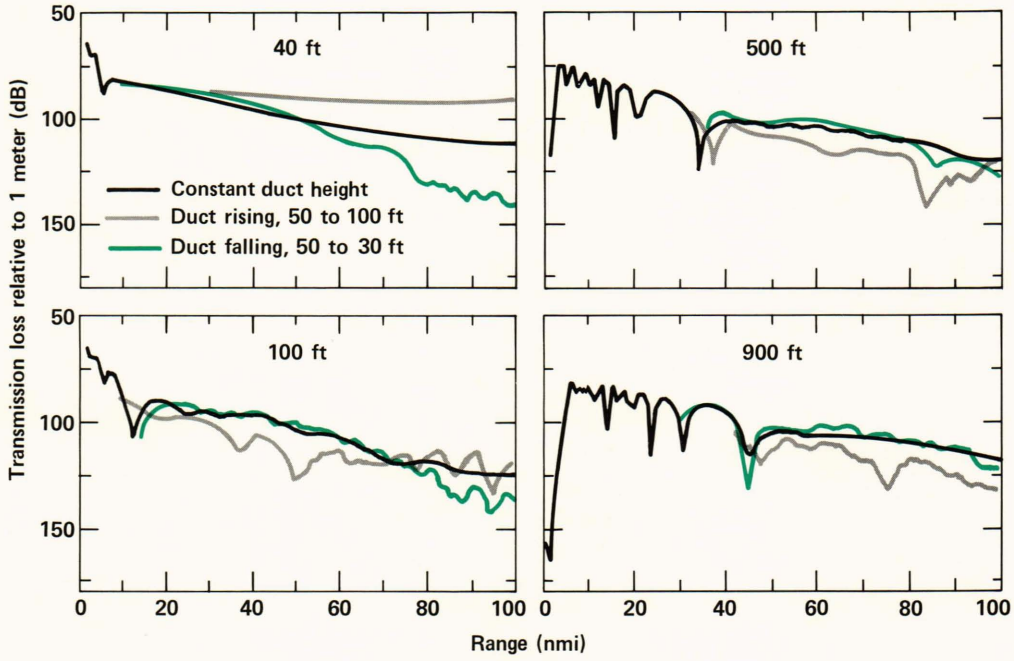

Figure 16 — Horizontal profiles of propagation loss in dB relative to 1 meter for a 3-gigahertz antenna at 100 feet. The profiles are given at the altitudes of (a) 40 feet, (b) 100 feet, (c) 500 feet, and (d) 900 feet for the evaporation ducts with constant height (black), falling height (blue), and rising height (gray).

through inhomogeneous media, with computational efficiency and accuracy as prime objectives. Better empirical observations of absorption and clutter backscatter are always desired. Boundary layer meteorology treats the physical effects in the troposphere that contribute to the refractive behavior. These effects include local atmospheric pressure forces and advection, Coriolis and large-scale synoptic forces, long- and short-wave radiation, boundary layer turbulence, and atmospheric and surface water content. Synoptic climatology provides the data from which the seasonal and diurnal effects can be surveyed. It also provides a connection between the migration of large upper air masses and elevated refractive layers. Physical oceanography treats the effects of ocean processes on surface temperature, surface heat flux, and moisture balance, which is vital to the understanding of the evaporation duct and tropospheric air circulation. This information is selectively integrated through systems analysis to provide a model of the troposphere that can be used to study the performance of each system under specific criteria.

We must appreciate that contributions to the understanding of anomalous propagation will come from a variety of sources. It is hoped that future analytical and testing programs will utilize this interdisciplinary approach to take peculiar observations out of the realm of folklore and to use the knowledge gained for practical purposes.

REFERENCES

[1]E. C. Brewer, *Brewer's Dictionary of Phrase and Fable*, Harper and Row, New York, p. 192 (1970).
[2]D. E. Kerr, *Propagation of Short Radio Waves,* McGraw-Hill, New York, p. 371 (1951).
[3]D. C. Livingston, *The Physics of Microwave Propagation,* Prentice-Hall, New Jersey, p. 106 (1970).
[4]W. P. Elliott, "The Growth of the Atmospheric Internal Boundary Layer," *Trans. Am. Geophys. Union* **39,** 1048-1054 (1958).
[5]S. H. Cho and J. R. Wait, "Analysis of Microwave Ducting in an Inhomogeneous Troposphere," *Pure Appl. Geophys.* **116,** 1118-1142 (1979).
[6]M. A. Leontovich and V. A. Fock, "Solution of the Problem of Propagation of Electromagnetic Waves Along the Earth's Surface by the Method of Parabolic Equation," *J. Phys. USSR* **10,** 13-23 (1946).
[7]R. H. Hardin and F. D. Tappert, "Application of the Split-Step Fourier Method to the Numerical Solution of Nonlinear and Variable Coefficent Wave Equations, " *SIAM Rev.* **15,** 423 (1973).

REFERENCES FOR PAGES 20-21

[A1]M. A. Leontovich and V. A. Fock, "Solution of the Problem of Propagation of Electromagnetic Waves Along the Earth's Surface by the Method of Parabolic Equation," *J. Phys. USSR* **10,** 13-23 (1946).
[A2]J. W. Sari and R. I. Joseph, "Tropospheric Propagation of Radiation for an Inhomogeneous Stratified Atmosphere," National Radio Science Meeting, Boulder, Colo. (14 Jan 1982).
[A3]S. T. McDaniel, "Propagation of Normal Modes in the Parabolic Approximation, " *J. Acous. Soc. Am.* **57,** 307-311 (1975).
[A4]M. A. Leontovich, "On the Approximate Boundary Conditions for an Electromagnetic Field on the Surface of Well-Conducting Bodies," in *Investigations of Propagation of Radio Waves,* B.A. Vedensky, ed. Academy of Science, Moscow, USSR (1948).
[A5]R.H. Hardin and F. D. Tappert, "Application of the Split-Step Fourier Method to the Numerical Solution of Nonlinear and Variable Coefficient Wave Equations," *SIAM Rev.* **15,** 423 (1973).